Effect of metallographic structure and machining process on the apatite-forming ability of sodium hydroxide- and heat-treated titanium

Toshiki Miyazaki[a,*], Takashi Sasaki[a], Yuki Shirosaki[a,b], Ken'ichi Yokoyama[c] and Masakazu Kawashita[d]

[a]Graduate School of Life Science and System Engineering, Kyushu Institute of Technology, Kitakyushu, Japan

[b]Frontier Research Academy for Young Researchers, Kyushu Institute of Technology, Kitakyushu, Japan

[c]Graduate School of Engineering, Kyushu Institute of Technology, Kitakyushu, Japan

[d]Graduate School of Biomedical Engineering, Tohoku University, Sendai, Japan

Corresponding author:

Toshiki Miyazaki

Graduate School of Life Science and Systems Engineering, Kyushu Institute of Technology,

2-4, Hibikino, Wakamatsu-ku, Kitakyushu 808-0196, Japan

Tel/Fax: +81-93-695-6025

E-mail: tmiya@life.kyutech.ac.jp

Abstract

Although titanium (Ti) is clinically used for hard tissue reconstruction, it has low bone-bonding ability, i.e. bioactivity. Materials able to deposit apatite on their surfaces within the body is considered to exhibit bioactivity. Effects of the metallographic structure and machining process of Ti on its apatite-forming ability remains unclear. In this study, Ti substrates subjected to various preheating and machining processes were then subjected to NaOH and heat treatments. The apatite-forming abilities of resulting Ti were examined in simulated body fluid (SBF). Preheating of the Ti decreased its reactivity with NaOH solution. When quenched or annealed Ti was subjected to NaOH and heat treatments, the induction period for apatite formation in SBF slightly increased. This was attributed to a decrease in sodium titanate and increase in rutile on the Ti surface after the treatments. Substrates subjected to wire-electrical-discharge machining did not form apatite. This was attributed to the inhibition of PO_4^{3-} adsorption on their surfaces following Ca^{2+} adsorption, which is an essential process for apatite nucleation. Contamination of Ti surface by components of the brass wire used in the machining contributed to the inhibition. The bioactivity of surface-modified Ti was therefore significantly affected by its thermal treatment and machining process.

Keywords: Titanium (Ti), NaOH and heat treatment, Apatite, Metallographic structure,

Machining, Bioactivity

1. Introduction

Titanium (Ti) and its alloys have excellent biological compatibility and fracture toughness. They are therefore clinically used for reconstructing hard tissue under loaded conditions, such as in artificial tooth roots and joints. However, achieving rapid bone-bonding bioactivity for Ti is difficult. Studies on bioactive ceramics suggest that forming bone-like apatite within the body is an essential requirement for bioactivity [1]. Long time durations are required to form apatite on as-received Ti [2,3]. Forming titanium oxide or hydroxide layers on Ti by surface modification has been extensively investigated to enhance apatite formation. NaOH and heat treatments [4], hydrogen peroxide and heat treatments [5], anodic oxidation [6], and autoclave treatment [7] have been proposed for such surface modification. The crystal structure of the titanium oxide [8], amount and acidity of Ti-OH groups [9,10], ability of Ca^{2+} to be released from Ti [11], and amount of surface lattice vacancies [12] have also been suggested as factors governing apatite formation in Ti-based materials.

The crystal structures of metal substrates can generally be controlled by their machining method and heat treatment history. Their crystal structures in turn govern their mechanical and biological properties. It was reported that roughening and oxide formation on the Ti surface by wire-electrical-discharge machining enhanced the activity of alkali phosphatase and osteocalcin [13,14]. Ti subjected to wire-electrical-discharge machining was also reported

4

to have a higher ability to form calcium phosphate in Hanks' solution, compared with as-polished Ti [15]. However, the effects of the crystal structure and machining process on the apatite forming ability of NaOH- and heat-treated Ti have not been fully examined. Clarifying these will yield information on optimal processing conditions for bone integration.

In this study, Ti substrates with different metallographic structures were prepared by various heat treatment and machining processes. Apatite formation on substrates subjected to NaOH and heat treatments was examined *in vitro* using simulated body fluid (SBF).

2. Materials and Methods

2.1. Crystal structural control of Ti

Ti (99.5%, Nilaco Co., Tokyo, Japan) was cut into rectangular samples of $10 \times 10 \times 1$ mm in size, using a shearing machine (FS-101D, Noguchi Press Co., Japan) and a wire electrical discharge machine (Mitsubishi Electronics, Tokyo, Japan). Some of the shear-machined substrates were heated to 1000 °C for 1 h in an electric furnace (KDF S-70, Denken Co. Ltd., Kyoto, Japan), and then immediately quenched in ultrapure water, or otherwise annealed at 800 °C for 5 h. Substrates were then polished with #120 SiC paper to remove the surface oxide layer, and ultrasonically washed in acetone for 30 min and then in ultrapure water for 30 min. Table 1 summarizes the different substrates and their various

treatments.

2.2. NaOH and heat treatments

Ti substrates were soaked in 5 mL of 5 M NaOH aqueous solution, and then mechanically agitated in a water bath (H-10, Taitec Co., Saitama, Japan) at 60 °C for 1 day. The agitating speed was fixed at 120 strokes/min. The substrates were then removed from solution, and gently washed with ultrapure water. They were then dried at 60 °C for 1 day, heated to 600 °C at 5 °C/min, retained at 600 °C for 1 h, and then allowed to cool in the furnace.

2.3. Soaking in SBF

Treated substrates were soaked in 30 mL of SBF containing the following inorganic ion concentrations (142.0 mM Na^+, 5.0 mM K^+, 2.5 mM Mg^{2+}, 147.8 mM Cl^-, 4.2 mM HCO_3^-, 1.0 mM HPO_4^{2-}, and 0.5 mM SO_4^{2-}) at 36.5 °C for various periods. The pH of the solution was buffered at 7.40 by 50 mM tris(hydroxymethyl)aminomethane and an appropriate amount of HCl. SBF was prepared according to the literature [16]. All reagents used for preparing SBF were purchased from Nacalai Tesque Inc., Kyoto, Japan. After soaking, the substrates were removed from the SBF, and then immersed in ultrapure water for 30 min to remove

6

excess water-soluble salts on their surface.

2.4. Characterization

Metallographic observations were performed as follows. Ti substrates before NaOH treatment were embedded in light-curing resin, and polished to a mirror-like surface using SiC papers of #120, #240, #500, #800, #1000, #1500, #2400 and #4000, and then using colloidal silica (40 nm), in this order. Finally, they were etched in a mixed solution containing 4.3 mass% of HF and 10.6 mass% of HNO_3 for 10 s. HF is a highly harmful chemical substance, so protection items were used in the experiment and waste solution was appropriately disposed after detoxifying by calcium compounds. Surfaces were observed using an optical microscope.

To analyze corrosion behavior, Ti substrates before NaOH treatment were embedded in light-curing resin and then polished using SiC paper of #120. Anodic polarization measurements were performed in 1 M NaOH by a potentiostat/galvanostat (HA-151A, Hokuto Denko Co., Tokyo, Japan) and function generator (HB-111, Hokuto Denko Co., Tokyo, Japan). Pt was used as the counter electrode, and the sweeping speed was fixed at 20 mV/min.

The surface structural changes of the substrates were characterized using scanning electron microscopy (SEM; Model S-3500N; Hitachi Co., Tokyo, Japan), energy dispersive

X-ray spectroscopy (EDX; Model EX-400; Horiba Co., Kyoto, Japan), thin-film X-ray diffraction (TF-XRD; MXP3V; Mac Science Ltd., Yokohama, Japan), and X-ray photoelectron spectroscopy (XPS, KRATOS AXIS-Nova, Shimadzu Co., Kyoto, Japan). In TF-XRD experiments, the incident beam was fixed at 1° against the surface of each substrate, with a scan rate of $0.02°·s^{-1}$. In XPS experiments, measured binding energies were corrected by referring to the C 1s binding energy of the methylene groups of hydrocarbon (284.6 eV) adsorbed on the substrate surface.

Surface zeta potentials of substrates in SBF were measured using a zeta-potential analyzer (ELS-Z, Otsuka Electronics Co., Osaka, Japan) with a connected box-like quartz cell. After substrates had been soaked in SBF for various periods, the surface of the substrate was placed on the quartz cell, and then flesh SBF and monitor particles (polyethylene latex, Otsuka Electronics Co.) were injected into the cell. To measure the surface zeta potential, the electrophoretic mobility of the monitor particles was measured using a laser Doppler method [17].

3. Results

Figure 1 shows the metallographic structures of Ti substrates subjected to different heat treatment and machining processes, before NaOH treatment. Substrates S and W were

composed of equiaxed crystals of 20–40 μm in size. The metallographic structure changed

significantly upon quenching or annealing. Namely, substrate S-Q precipitated needle-like

crystals (actually platelet crystals) with a Widmanstatten pattern. Substrate S-A showed

significant crystal growth, with crystals of 200–400 μm in size. This tendency was consistent

with previous studies [18,19].

Results of anodic polarization in 1 M NaOH solution are shown in Fig. 2. Substrates S

and W showed increased current densities at around –0.2 V due to hydrogen generation, and

at around 0.6 V due to oxygen generation. Substrates S-Q and S-A showed minimal (if any)

increased current densities in these regions. The maximum current density was much higher

in substrates S and W (more than 1 A·m^{-2}) than in substrates S-Q and S-A (around 0.1 A·m^{-2}).

This indicted that substrates S-Q and S-A had higher corrosion resistances than substrates S

and W.

Figure 3 shows TF-XRD patterns of the substrates after NaOH treatment and

subsequent heat treatment. After NaOH treatment, broad peaks assigned to amorphous sodium

titanate were observed at 24–28° 2θ. These peak were slightly stronger in the TF-XRD

patterns of substrates S and W, than in those of substrates S-Q and S-A. After subsequent heat

treatment, peaks assigned to rutile and $Na_2Ti_5O_{11}$ as well as those of Ti were observed in the

TF-XRD patterns of all samples. The ratio of $Na_2Ti_5O_{11}$ / rutile calculated from the TF-XRD

peak intensities (peak position: $Na_2Ti_5O_{11}$ 24.5° 2θ, rutile 27.5° 2θ) in Fig. 3 decreased in the order: W > S > S-Q > S-A. These results suggested that amorphous sodium titanate formation by NaOH treatment was suppressed in the quenched and annealed samples.

Figure 4 shows O1s XPS spectra of the surfaces of shear and wire machined samples subjected to NaOH and heat treatments. Peaks around 530 and 532 eV corresponds to Ti-O bond, and Ti-OH or adsorbed water, respectively. Each peak intensity was almost similar for both the specimens. This indicates that there is no significant difference in chemical state of surface oxide and hydroxide.

Figure 5 shows TF-XRD patterns of substrates subjected to NaOH and heat treatments after soaking in SBF for 7 days. Broad peaks assigned to low-crystallinity apatite were observed at 26 and 32° 2θ in the TF-XRD patterns of all substrates, except for substrate W. SEM images of the same substrates are shown in Fig. 6. Spherical particles almost completely covered the surface of substrate S, and partially covered the surfaces of substrates S-Q and S-A, but not for substrate W. The apatite formation behaviors are summarized in Table 2, taking into account the other soaking periods. The rate of apatite formation decreased in the order: S > S-Q ≈ S-A > W.

Figure 7 shows EDX spectra of the surfaces of shear- and wire-electrical-discharge machined substrates subjected to NaOH and heat treatments, which were soaked in SBF for 7

days. Strong Ca and P peaks were detected in the spectrum of substrate S. A much weaker Ca

peak was detected in the spectrum of substrate W. This suggested that calcium titanate rather

than calcium phosphate formed on the surface of substrate W in SBF.

Figure 8 shows changes in the zeta potentials of the surfaces of shear- and

wire-electrical-discharge machined substrates subjected to NaOH and heat treatments, after

soaking in SBF for various periods. The zeta potential initially decreased and then

subsequently increased with increasing soaking time for substrate S. The zeta potential was

largely constant with increasing soaking time for substrate W.

4. Discussion

The heat treatment of Ti improved its corrosion resistance against NaOH solution, as

shown in Fig. 2. This conclusion was supported by the results in Fig. 3 showing suppressed

sodium titanate formation. Grain growth upon heat treatment would have enhanced the

corrosion resistance, because of the decrease in the amount of reactive grain boundaries, as

shown in Fig. 1. This assumption was supported by nanoscale grain-sized Ti (90 nm)

reportedly showing a lower corrosion resistance against 0.9% NaCl solution than microscale

grain-sized Ti (21 μm) [20].

When pre-heat-treated Ti substrates were subjected to NaOH and heat treatments, the induction time for apatite formation in SBF was slightly increased. The amounts of sodium titanate formed on substrates S-Q and S-A during NaOH and heat treatments were lower than those formed on substrates S and W. Therefore, the diffusion of oxygen from the atmosphere into the bulk substrates would have increased. This would have enhanced the formation of rutile during subsequent heat treatment. Sugino *et al*. reported that rutile formed merely by heating the Ti, and that controlling the surface topology such as fabricating grooves was necessary to impart Ti with apatite-forming ability [21]. This suggested that a rutile-rich surface had a low apatite-forming ability. Similar phenomenon would have occurred in the present substrates.

Wire-electric-discharge machined Ti was similar to shear-machined Ti in terms of metallographic and crystal structure. XPS spectra in Fig. 4 indicated no differences in the surface chemical states of Ti-OH between substrates machined by these two processes, which reportedly affects apatite-forming ability [9,10]. Nevertheless, wire-electric-discharge machined Ti did not form apatite in SBF after 7 days. Behavior of variation in zeta potential on S and W in SBF was different (See Fig. 8). Mechanism of the apatite formation on NaOH- and heat-treated Ti has been explained as follows. Original sodium titanate has a negative zeta potential [22]. After soaking in SBF, the surface zeta potential of NaOH- and heat-treated Ti

12

increased due to Ca^{2+} adsorption, and then decreased due to subsequent PO_4^{3-} adsorption to form amorphous calcium phosphate, which is a precursor to apatite [23]. On the basis of these findings, the surface reaction on substrates S and W in SBF can be interpreted as follows. First, Ca^{2+} adsorbed on both substrates within the first 1 h. PO_4^{3-} then adsorbed on substrate S, but not on substrate W. This conclusion was supported by the EDX spectra in Fig. 7. Wire-electrical-discharge machining therefore inhibited the Ti surface from adsorbing PO_4^{3-} in SBF, although the reason for this phenomena has not been clarified.

Fujimori *et al.* reported that Ti machined with Ti wire deposited calcium phosphate crystals on its surface in Hanks' solution [15]. Brass wire was used for machining in the current study. Therefore, it was assumed that the Ti substrate was contaminated with components of the brass wire (Cu and Zn), which therefore inhibited apatite formation. In a similar phenomenon, Shozui *et al.* reported that anatase-type TiO_2 thin films coated on stainless steel and alumina did not form apatite in SBF. This was attributed to Al and Cr in the substrate being incorporated into the anatase layer [24]. A detailed mechanism of such surface contamination should be further investigated in the future.

5. Conclusion

The apatite-forming ability of bioactive Ti prepared by NaOH- and heat treatments was significantly affected by its metallographic structure and machining process. Thus, both surface modification and the Ti machining process should be considered when developing bone-integrating biomaterials.

References

1. Kokubo T, Kim HM, Kawashita M. Novel bioactive materials with different mechanical properties. Biomaterials 2003;24:2161-2175.

2. Hanawa T, Ota M. Calcium phosphate naturally formed on titanium in electrolyte solution. Biomaterials 1991;12:767–774.

3. Narushima T. Titanium and its alloys as biomaterials. J. Japan Inst. Light Metals 2005;55:561–565 (in Japanese).

4. Kim HM, Miyaji F, Kokubo T, Nakamura T. Preparation of bioactive Ti and its alloys via simple chemical surface treatment. J. Biomed. Mater. Res. 1996;32:409-417.

5. Wang XX, Hayakawa S, Tsuru K, Osaka A. A comparative study of in vitro apatite deposition on heat-, H_2O_2-, and NaOH-treated titanium surfaces. J. Biomed. Mater. Res. 2001;54:172-178.

6. Yang BC, Uchida M, Kim HM, Zhang X, Kokubo T. Preparation of bioactive titanium metal via anodic oxidation treatment. Biomaterials 2004;25:1003–1010.

7. Kawashita M, Matsui N, Miyazaki T and Kanetaka H. Effect of autoclave and hot water treatments on surface structure and *in vitro* apatite-forming ability of NaOH- and heat-treated bioactive titanium metal. Mater. Trans. 2013;54:811-816.

8. Uchida M, Kim HM, Kokubo T, Fujibayashi S and Nakamura T. Structural dependence of apatite formation on titania gels in a simulated body fluid. J. Biomed. Mater. Res. A 2003;64:164-170.

9. Obata A, Zhai T and Kasuga T. Apatite-forming ability on titanium surface modified by hydrothermal treatment and ultraviolet irradiation. J. Mater. Res. 2008;23:3169-3175.

10. Hayakawa S, Matsumoto Y, Uetsuki K, Shirosaki Y, Osaka A. In vitro apatite formation on nano-crystalline titania layer aligned parallel to Ti6Al4V alloy substrates with sub-millimeter gap. J. Mater. Sci.: Mater. Med. 2015;26:190.

11. Kizuki T, Takadama H, Matsushita T, Nakamura T, Kokubo T. Preparation of bioactive Ti metal surface enriched with calcium ions by chemical treatment. Acta Biomater. 2010;6:2836-2842.

12. Hashimoto M, Hayashi K, Kitaoka S. Enhanced apatite formation on Ti metal heated in PO_2-controlled nitrogen atmosphere. Mater. Sci. Eng. C 2013;33:4155-4159.

13. Otsuka F, Kataoka Y, Miyazaki T. Enhanced osteoblast response to electrical discharge machining surface. Dent. Mater. J. 2012;31:309-315.

14. Yang TS, Huang MS, Wang MS, Lin MH, Tsai MY, Wang PY, Effect of electrical discharging on formation of nanoporous biocompatible layer on Ti-6Al-4V alloys. Implant Dent. 2013;22:374-379.

15. Fujimori S, Suzuki M, Shibata Y, Fujino S and Miyazaki T. Titanium plates treated by wire-type electric discharge machining promote the precipitation of calcium phosphate on their surfaces in electrolyte solution. J. Showa Univ. Dent. Soc. 1997;17:362-367 (in Japanese).

16. Cho SB, Kokubo T, Nakanishi K, Soga N, Ohtsuki C, Nakamura T, Kitsugi T and Yamamuro T. Dependence of Apatite Formation on Silica Gel on Its Structure: Effect of Heat Treatment. J. Am. Ceram. Soc. 1995;78:1769-1774.

17. Clogston JD, Patri AK. Zeta Potential Measurement. In: McNeil SE, editor. Characterization of Nanoparticles Intended for Drug Delivery. Switzerland: Springer; 2011. pp 63-70.

18. Nishiyama Z, Oka M and Nakagawa H. The Electron Microscope Structure and Lattice Defects of Martensite in Commercially Pure Titanium. J. Japan Inst. Metals 1965;29:133-138 (in Japanese).

19. Nishimura T, Fukuda M. Recrystallization behavior of Ti and its alloys. Tetsu-to-Hagane 1984;70:1898-1905 (in Japanese).

20. Garbacz H, Pisareka M and Kurzydłowski KJ. Corrosion resistance of nanostructured titanium. Biomol. Eng. 2007;24:559–563.

21. Sugino A, Tsuru K, Hayakawa S, Kikuta K, Kawachi G, Osaka A and Ohtsuki C. Induced deposition of bone-like hydroxyapatite on thermally oxidized titanium substrates using a spatial gap in a solution that mimics a body fluid. J. Ceram. Soc. Japan 2009;117:515-520.

22. Grover IS, Singh S and Pal B. The preparation, surface structure, zeta potential, surface charge density and photocatalytic activity of TiO_2 nanostructures of different shapes. Appl. Surf. Sci. 2013;280:366–372.

23. Kim HM, Himeno T, Kawashita M, Lee JH, Kokubo T and Nakamura T. Surface potential change in bioactive titanium metal during the process of apatite formation in simulated body fluid. J. Biomed. Mater. Res. 2003;67A:1305–1309.

24. Shozui T, Tsuru K, Hayakawa S, Shirosaki Y, Osaka A. A XPS study on potential suppression factors of suppressing in vitro apatite formation on anatase films prepared on various substrates. Surf. Coat. Tech. 2009;203:2181-2185.

Table 1   Ti substrates analyzed in this study

Sample	Machining	Heat treatment		Cooling
		Temperature	Time	
S	Shear	None	None	None
S-Q	Shear	1000°C	1 hour	Quench
S-A	Shear	800°C	5 hours	Anneal
W	Wire electrical discharge	None	None	None

Table 2   Apatite formation on Ti substrates in SBF

Sample	Soaking time		
	3 days	5 days	7 days
S	X	O	O
S-Q	X	X	O
S-A	X	X	O
W	X	X	X

Figure captions

Fig. 1 Microstructures of Ti substrates subjected to different heat treatment and machining processes, before NaOH treatment.

Fig. 2 Anodic polarization curves of Ti substrates subjected to different heat treatment and machining processes in 1 M NaOH solution.

Fig. 3 TF-XRD patterns of Ti substrates subjected to various NaOH and heat treatments.

Fig. 4 O1s XPS spectra of the surfaces of shear and wire machined samples subjected to NaOH and heat treatments.

Fig. 5 TF-XRD patterns of Ti substrates subjected to various NaOH and heat treatments, which were soaked in SBF for 7 days.

Fig. 6 SEM images of Ti substrates subjected to various NaOH and heat treatments, which were soaked in SBF for 7 days.

Fig. 7 EDX spectra of the surfaces of shear- and wire-electrical-discharge machined substrates subjected to various NaOH and heat treatments, which were soaked in SBF for 7 days.

Fig. 8 Changes in zeta potentials of the surfaces of shear- and wire-electrical-discharge machined substrates subjected to various NaOH and heat treatments, which were soaked in

SBF for various periods (n=4).

S

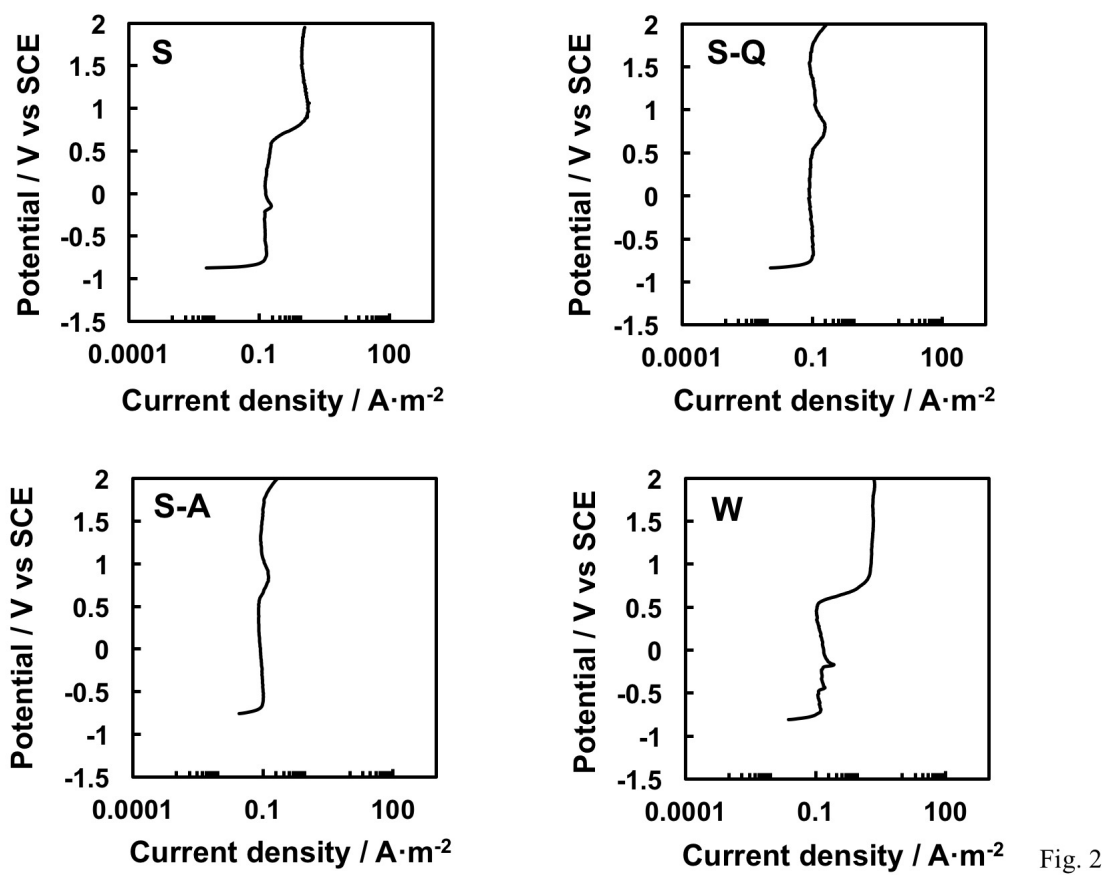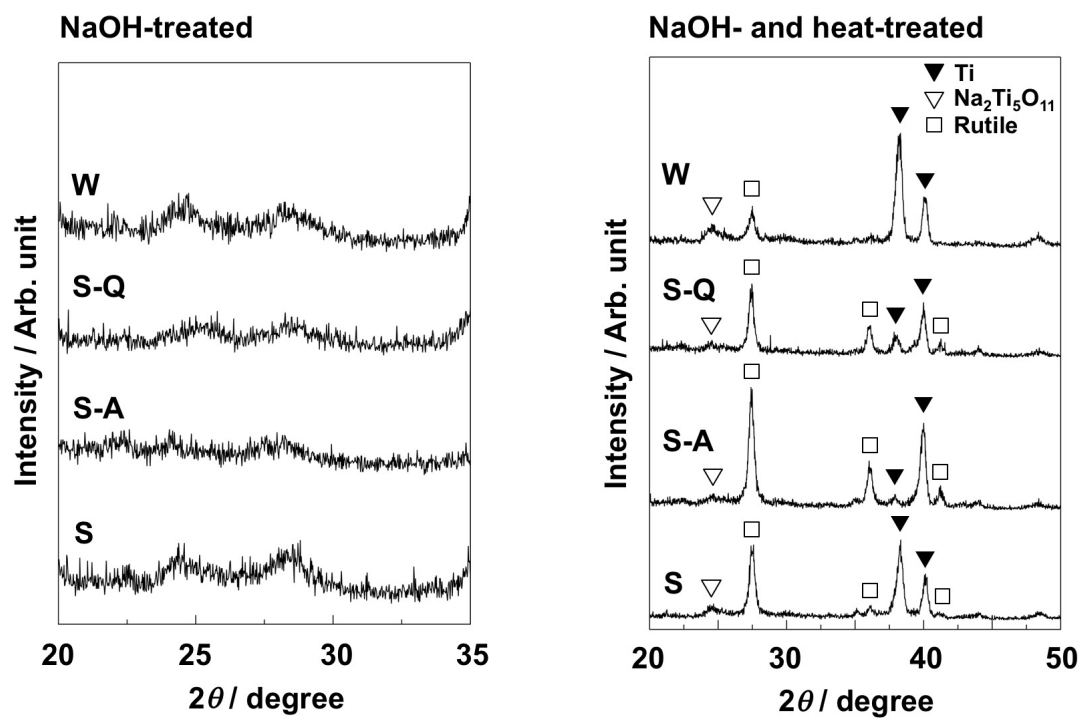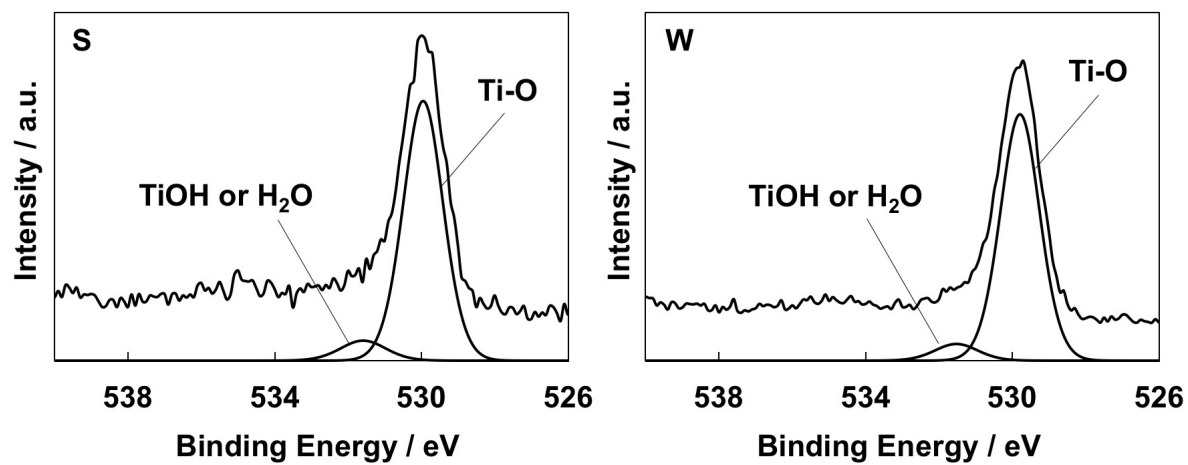**S-Q**

S-A

W

Fig. 1

Fig. 2

NaOH-treated

NaOH- and heat-treated

Fig. 3

Fig. 4

Fig. 5

S

S-Q

S-A

W

20 µm

20 µm

20 µm

20 µm

Fig. 6

Fig. 7

Fig. 8